RSC Advances

PAPER

View Article Online
View Journal | View Issue

Cite this: *RSC Adv.*, 2025, **15**, 3219

Fabrication and characterization of an Al_2O_3/OPSZ/Al_2O_3 barrier film on a PEN substrate *via* PEALD and spray-spin coating techniques

Xiaojie Sun and Wei Feng *

Received 27th November 2024
Accepted 14th January 2025

DOI: 10.1039/d4ra08383k

rsc.li/rsc-advances

One of the main drawbacks of the current flexible devices is the lack of a thin-film encapsulation with superior moisture barrier performance, light transmittance and mechanical flexibility. In this study, an inorganic/organic/inorganic composite film was fabricated on a 10 cm × 10 cm polyethylene naphthalate (PEN) substrate, which consisted of two inorganic layers of Al_2O_3 with an organic layer of organic polysilazane (OPSZ) in between. Al_2O_3 was deposited *via* plasma-enhanced atomic layer deposition (PEALD) with a thickness of about 40 nm. Approximately 200 nm thick OPSZ was prepared using the spray-spin coating method. The multilayer film exhibited outstanding optical transmittance (>90%) and an extremely low water vapor transmission rate (WVTR) (4.6×10^{-5} g per m^2 per day, 38 °C, 90% RH), which is two orders of magnitude lower than that of the corresponding single-layer Al_2O_3 film. Moreover, the introduction of an organic layer helped the Al_2O_3/OPSZ/Al_2O_3 film to exhibit good tensile and bending resistance. Thus, the multilayer film may find applications in the encapsulation of flexible devices.

1. Introduction

Film encapsulation is an important technical assurance for the commercial application of flexible devices, such as flexible displays and flexible solar cells. Encapsulation barrier films play a crucial role in preventing the devices from being permeated by moisture and oxygen.[1–5] In particular, water causes more severe degradation than oxygen, and hence, effective protection from water vapor is crucial during the encapsulation of flexible electronic devices.[6–8]

Metal foils are potential barrier materials owing to their good mechanical properties, low cost, ease of formability, and good barrier properties.[9] However, barrier films for flexible electronic devices require transparency. Glass-based materials display good barrier properties and transparency, but their mechanical properties and processibility are undesirable.[10] Alternatively, metal oxide deposited onto transparent and soft substrates affords nearly all requirements for flexible devices.[11] Metal oxides, such as Al_2O_3, MgO and ZrO_2, grown by atomic layer deposition (ALD) are reported to provide excellent moisture barrier properties.[12–14] Further, alternating inorganic laminates, such as Al_2O_3/MgO,[15] Al_2O_3/ZrO_2 [16] and Al_2O_3/HfO_2,[17] have shown superior barrier performance over corresponding single-layer films. However, during the fabrication process, microcracks or pinholes might be introduced, inevitably providing pathways for the penetration of oxygen and moisture.[18,19] To enhance the barrier performance, the total number of dyads and the thickness of the layers are often increased. However, shortcomings such as cracking occurring in films and low optical transmittance may still persist. Inserting an organic layer into neighboring inorganic layers can decouple defects or pinholes and prolong permeation pathways, and this appears to be a promising strategy.[20–23] Van de Weijer *et al.*[24] reported a thin-film encapsulation stack consisting of two inorganic barrier layers separated by an organic planarization layer. The 1.5-dyad structure exhibited a significant delay in the formation of black spots when applied on an OLED display. Duan *et al.*[25] fabricated multiple stacked layers of Al_2O_3/alucone film on a flexible PET substrate and delivered an extremely low water vapor transmission rate (WVTR) (9.94×10^{-5} g per m^2 per day). Previous studies have demonstrated the synergetic effect of hybrid films on the barrier properties. However, among the various fabrication protocols, achieving cost-effective manufacturing of multilayer architecture and realizing them as smooth, stretchable, durable barrier films are still challenging.

In this study, we developed an inorganic/organic/inorganic composite film. Al_2O_3, which has the best water vapor barrier performance among the inorganic oxides, was chosen as the inorganic sublayer. Organic polysilazane (OPSZ) was chosen as the organic sublayer owing to its high transparency and thermal stability. A multilayer film consisting of two inorganic Al_2O_3 layers and an intermediate OPSZ layer was fabricated. The first Al_2O_3 layer was prepared by plasma-enhanced atomic layer deposition (PEALD) operated at a low deposition temperature, allowing a high quality Al_2O_3 layer with excellent barrier performance. An adjacent OPSZ layer was prepared using the

School of Materials Science and Engineering, Tianjin University, Tianjin, 300350, China. E-mail: weifeng@tju.edu.cn

spray-spin coating method. In general, spin coating is suitable for the uniform coating of small samples. A process that combines spray coating and spin coating can produce nanoscale polymer films with highly uniform thickness over a large substrate area. Afterwards, the plasma treatment was used on the hydrophobic OPSZ surface to provide rich nucleation sites for the deposition of another Al_2O_3 layer. The elemental content and water contact angle (WCA) verified the changes in the surface characteristics after plasma treatment. A structural analysis was carried out, and the WVTR performance and optical transmittance of the developed multilayer film were evaluated. The obtained results demonstrated that multilayer film exhibits better performance than single-layer Al_2O_3 film. This work also provides insights into optimizing performance by modulating a hybrid structure.

2. Experimental section

2.1 Preparation of multilayer barrier films

The PEN/Al_2O_3/OPSZ/Al_2O_3 multilayer films were prepared on a polyethylene naphthalate (PEN) substrate with a thickness of 100 μm (DuPont Tejin films). The Al_2O_3 layer was grown in a Picosun R-200 ALD reactor using trimethylaluminium (TMA) and O_2 plasma at 120 °C. For each ALD cycle, 0.1 s exposure to TMA vapor, 6 s of N_2-purge, 26 s exposure to O_2 plasma, and 6 s of Ar-purge were applied in sequence. The intensity of the O_2 plasma generator was 2700 W. The growth rate of Al_2O_3 was approximately 0.124 nm per cycle. The spray-spin coating method[26] was used to prepare the nanoscale OPSZ (Durazane®1500, Merck) layer. In detail, 1 mL of OPSZ solution (20% solid content) was sprayed on the (ALD-deposited PEN/Al_2O_3) substrate at room temperature, followed by 60 s of spin coating. The rotation speed of the spin coating varied from 500 to 5000 rpm. The PEN/Al_2O_3/OPSZ film was cured at 80 °C for 2 hours. An 8 min plasma treatment was then performed to tune the wettability of the as-cured OPSZ film, in which the plasma power was set at 250 W. After that, the second layer of Al_2O_3 was deposited using the same ALD process conditions described above. Fig. 1 is a schematic of the multilayer film structure with information on the thickness of each layer.

2.2 Characterization of the barrier films

The microstructures of the films at varying preparation steps were characterized by applying a Scanning Electron Microscope (SEM, Nova NanoSEM 450, FEI Company). The surface morphology of the OPSZ prepared at different rotation speeds was captured using a 3D laser scanning microscope (VK-X1000, Keyence). The surface contact angle of the films was determined using a contact angle meter (DSA100, KRUSS). The surface elemental composition was measured using energy-dispersive X-ray spectroscopy (EDS) and X-ray photoelectron spectroscopy (XPS) (Escalab 250Xi, Thermo Scientific). The cross-sectional morphology of the film was observed using a Transmission Electron Microscope (TEM, JEM ARM200F, JEOL). Before TEM imaging, site-specific milling was performed by applying the focused ion beam (FIB) technique. The surface morphology and roughness of the films were evaluated using atomic force microscopy (Dimension ICON, Bruker). The optical transmittance of the films was measured using a spectrophotometer (UV-3600, Shimadzu) in the wavelength range of 400–1200 nm. The WVTR of the films with a sample size of about 10 cm × 10 cm was obtained using MOCON Aquatran 3 (Aquatran model 3, MOCON Inc., USA) at 38 °C and 90% relative humidity (RH). The fatigue tensile test method was used to study the flexibility of the barrier films. The number of tensile cycles was 100, and the tensile strain increased from 1% to 5%. In the bending test, the bending strain is calculated from the bending radius of the film. The formula is as follows: $\varepsilon = (t_1 + t_2)/2r$, where t_1 and t_2 are the thicknesses of the substrate and coating, respectively, and r is the bending radius. An ultra-depth 3D microscope (DSX510, OLYMPUS) was used to observe the changes in the surface topography of the samples.

3. Results and discussion

3.1 Microscopic morphology of the Al_2O_3 layer

In this work, Al_2O_3 layers were deposited by PEALD at 120 °C.[27] Fig. 2(a) shows the surface SEM image of the first Al_2O_3 layer deposited on the PEN substrate. The Al_2O_3 layer shows a homogeneous, smooth surface. Fig. 2(b) shows a cross-sectional SEM image of the PEN/Al_2O_3 film obtained after 350 ALD cycles. The Al_2O_3 layer thickness is about 44.7 nm, corresponding to an ALD growth rate of 0.124 nm per cycle. The number of ALD cycles was fixed at 350 for the Al_2O_3 layer deposition in the subsequent preparation of the Al_2O_3/OPSZ/Al_2O_3 multilayer barrier films.

3.2 Microscopic morphology of the OPSZ layer

The spray-spin coating method was used to prepare the nanoscale OPSZ layer. To determine the optimum coating

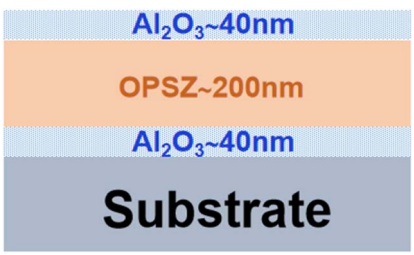

Fig. 1 Schematic of the multilayer barrier film.

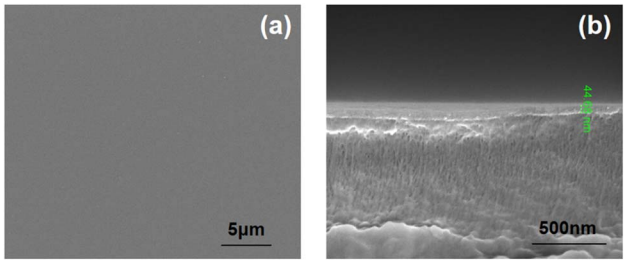

Fig. 2 Surface (a) and cross-sectional (b) SEM images of the Al_2O_3 film.

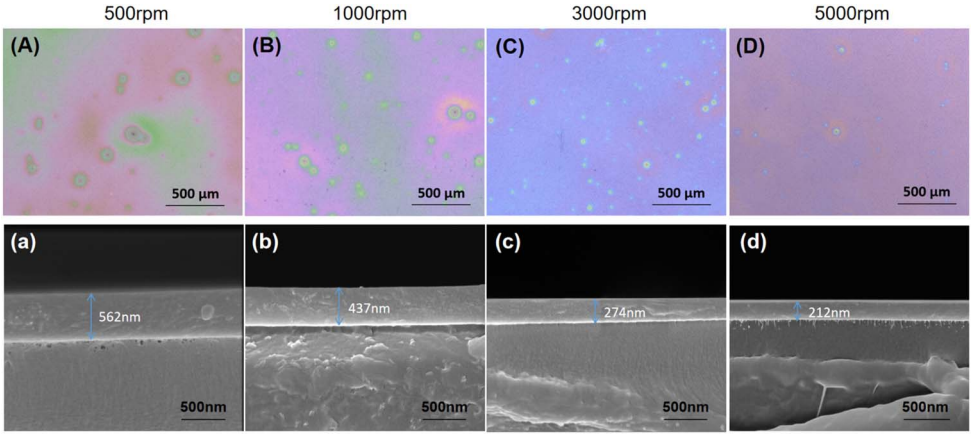

Fig. 3 Optical microscope images (A)–(D) and SEM cross-sectional images (a)–(d) of OPSZ layers on PEN substrate.

conditions, OPSZ layers were first prepared on a PEN substrate by varying the rotation speed in the range of 500–5000 rpm. A 3D laser scanning microscope was used to investigate the uniformity of the OPSZ films. As shown in Fig. 3(A)–(D), the OPSZ layer prepared with a rotation speed of 5000 rpm yields the smoothest surface. Besides, the thickness of the OPSZ layer decreases as the rotation speed increases, and the downward trend in film thickness levels off at rotation speeds above 3000 rpm. When the rotation speed reaches 5000 rpm, the thickness of the OPSZ layer is evaluated to be about 210 nm (Fig. 3(d)). A rotation speed of 5000 rpm was used in the subsequent spray-spin coating preparation of the OPSZ layer in the multilayer films.

3.3 Changes in PEN/Al_2O_3/OPSZ film surface with plasma treatment

OPSZ layer was coated on the surface of PEN/Al_2O_3 film. The prepared PEN/Al_2O_3/OPSZ film was then cured at 80 °C for 2 hours before plasma treatment. Water contact angle (WCA) measurements were taken on the as-cured and plasma treatment films. Fig. 4(a) shows that the OPSZ layer before plasma treatment shows a generally hydrophobic character with a contact angle of around 93°. In general, hydrophobic surfaces have low surface energy,[28] which is not conducive to nucleation during PEALD.[29,30] As shown in Fig. 4(b), a contact angle of around 0° is observed, indicating that a complete wetting surface has been achieved after O_2 plasma treatment. Fig. 4(c)–(f) further shows the effect of storage time on the WCA values on the OPSZ surface; the plasma-treated PEN/Al_2O_3/OPSZ film retains relative hydrophilicity after 7 days of storage time. It is thus demonstrated that plasma treatment is an effective protocol for rendering a hydrophilic surface and providing nucleation sites for the ALD process.

Fig. 5 shows the surface elemental compositions of films containing as-cured OPSZ layers measured by Energy Dispersion Spectroscopy (EDS). After plasma treatment, the oxygen content increases as shown in Fig. 5, indicating that oxygen-containing groups were introduced onto the surface of the OPSZ layer. The introduced functionalities improved the surface hydrophilicity. However, it is found that the increase in the oxygen element is relatively low. This is mainly because the

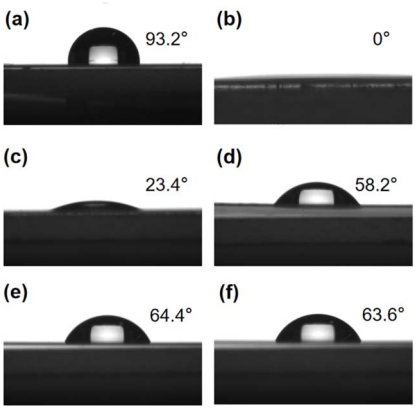

Fig. 4 Images of contact angle before (a) and after (b)–(f) plasma treatment: 0 day (b), 1 day (c), 3 days (d), 5 days (e), and 7 days (f) storage time after treatment.

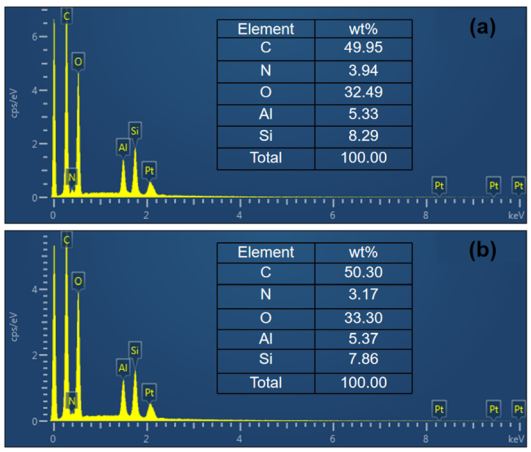

Fig. 5 EDS results of the OPSZ surface before (a) and after (b) plasma treatment.

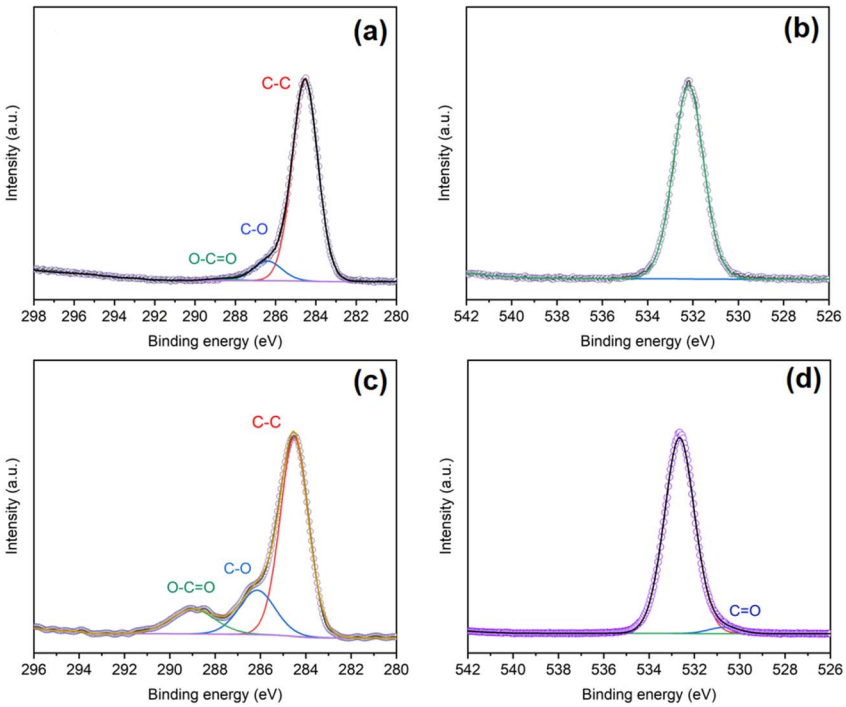

Fig. 6 C 1s and O 1s spectra of the OPSZ surface before (a) and (b) and after (c) and (d) plasma treatment.

plasma treatment is confined to only a few nanometers at the surface.

Fig. 6(a) and (c) show the C 1s high-resolution spectra of the OPSZ surface before and after plasma treatment, respectively. Compared with untreated OPSZ, plasma-treated OPSZ surface shows increased C–O and O–C═O/C–C ratios. Fig. 6(b) and (d) compare the O 1s high-resolution spectra of the OPSZ surface before and after treatment, respectively. A peak of O═C (530.7 eV) is detected in the treated OPSZ surface. Simultaneously, the binding energy of O 1s shifts from 532.2 eV to 532.6 eV, suggesting the presence of hydroxyl groups. The above analysis indicates that oxygen containing groups, such as O–C═O, C–O, and OH, have been successfully introduced on the OPSZ surface after the treatment.

3.4 Structure and properties of Al_2O_3/OPSZ/Al_2O_3 film

Fig. 7 shows a HRTEM image of the Al_2O_3/OPSZ/Al_2O_3 film on the PEN substrate. The film consists of a 44.76 nm-thick Al_2O_3

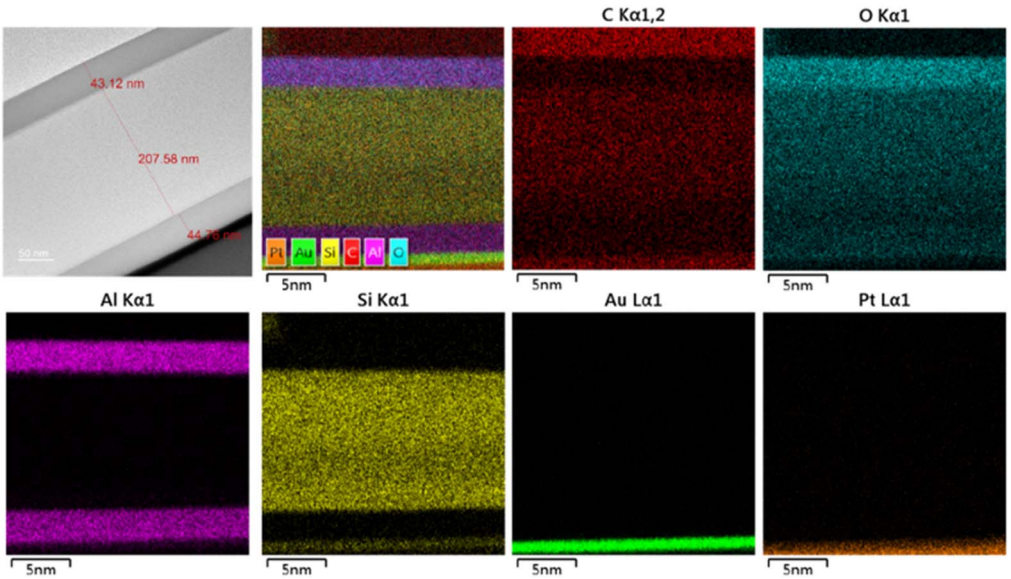

Fig. 7 HRTEM cross-sectional image and EDS mapping of the Al_2O_3/OPSZ/Al_2O_3 three-layer barrier film.

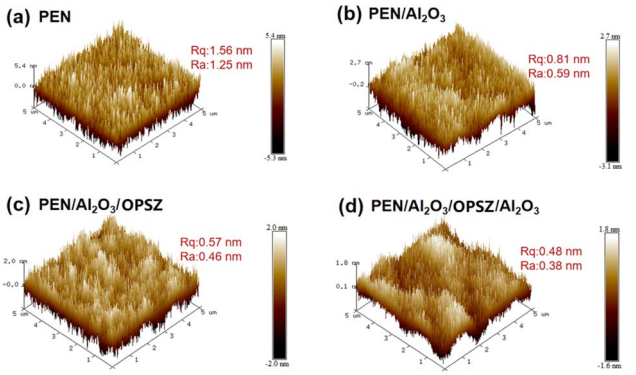

Fig. 8 AFM images and surface roughness values of (a) PEN, (b) PEN/Al_2O_3, (c) PEN/Al_2O_3/OPSZ, and (d) PEN/Al_2O_3/OPSZ/Al_2O_3.

layer, a 207.58 nm-thick OPSZ layer and another 43.12 nm-thick Al_2O_3 layer. The interfaces of PEN/Al_2O_3 and OPSZ/Al_2O_3 layers are well-defined. It is known that grain boundaries in crystalline layers are potential pathways for water vapor diffusion. Notably, the Al_2O_3 thin layer displays a continuous, homogeneous, and amorphous structure, minimizing the pathways for water permeating. From the mapping images, it is clearly observed that the Al and Si elements are uniformly distributed within the Al_2O_3 and OPSZ layers, respectively. The O element is distributed throughout the whole barrier film, while the C element is mainly distributed in the OPSZ layer. Both Au and Pt elements are artificially plated to protect the sample surface.

The surface smoothness of the bare PEN and different barrier films is measured by AFM over a scanned area of 5 μm × 5 μm. As shown in Fig. 8, the average surface roughness (R_a) for bare PEN is 1.25 nm. Upon deposition of the first Al_2O_3 layer, the surface roughness of the PEN/Al_2O_3 film decreases noticeably to 0.59 nm. Coating the OPSZ layer onto the above film results in further surface smoothing (R_a = 0.46 nm) (Fig. 8(c)). Thus, both the Al_2O_3 and OPSZ layers contribute to roughness reduction, which is conducive to the growth of a dense and pinhole-free Al_2O_3 surface layer of the multilayer barrier film. As expected, the subsequent Al_2O_3/OPSZ/Al_2O_3 barrier film shows a desired minimal R_a of 0.38 nm (Fig. 8(d)).

The WVTR was measured using MOCON Aquatran 3 to investigate the barrier properties of the films with regards to moisture. Unlike the small sample size of the Ca test, the size of the sample tested on MOCON equipment is as large as 10 cm × 10 cm. The WVTR for the pristine PEN substrate film is measured to be 1.3 g per m^2 per day, which is consistent with the reported results.[31] As shown in Fig. 9(a), the 350-cycle deposited PEN/Al_2O_3 thin film exhibits a WVTR value of 1.26 × 10^{-3} g per m^2 per day. As the deposition cycles increase to 700, the WVTR value of the PEN/Al_2O_3 film increases to 2.54 × 10^{-2} g per m^2 per day. The increased WVTR value could be ascribed to the propagation of defects. The introduction of an OPSZ layer on PEN/Al_2O_3 leads to a sharply decreased WVTR value (3.79 × 10^{-4} g per m^2 per day). Finally, after the ALD deposition of an additional layer of Al_2O_3, the multilayer film exhibits the lowest WVTR value of 4.6 × 10^{-5} g per m^2 per day, which is 2–3 orders of magnitude lower than that of a single Al_2O_3 film.

Optical properties are extremely important for barrier film for flexible devices. Normally, a light transmittance of higher than 90% is required for flexible electronic device encapsulation.[32] The optical transmittance as a function of wavelength for different barrier structures was measured by applying a UV-visible spectrophotometer, and the transmittance spectra are shown in Fig. 9(b). PEN/Al_2O_3/OPSZ and multilayer films show average transmittance values of 91.4% and 90.1% between 400 and 1200 nm wavelengths, respectively, which are more transparent than those of bare PEN substrate (Tr 87.5%) and PEN/Al_2O_3 film (Tr 88.5%). This demonstrates that the introduction of the OPSZ polymer layer can effectively prevent light scattering owing to its lower surface roughness, resulting in a higher transmittance of the multilayer films.

A schematic illustration of the reduced WVTR of the multilayer film compared to the neat Al_2O_3 film is presented in Fig. 10. First, the introduction of the OPSZ layer can help to achieve a flattened surface.[33] Meanwhile, the organic layer is known to decouple defects in Al_2O_3 layers, thereby preventing direct penetration through defect sites. Moreover, diffusion lag

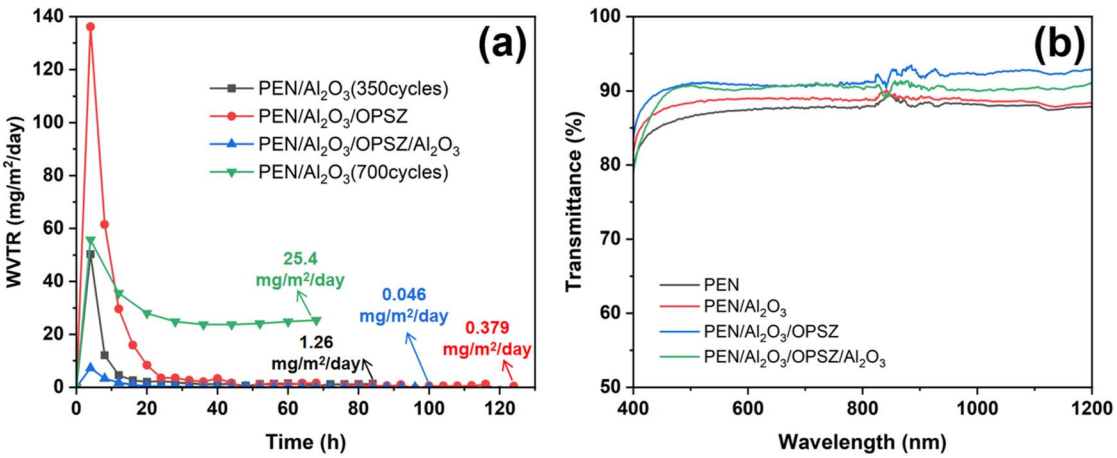

Fig. 9 WVTR values (a) and optical transmittance (b) of different barrier films.

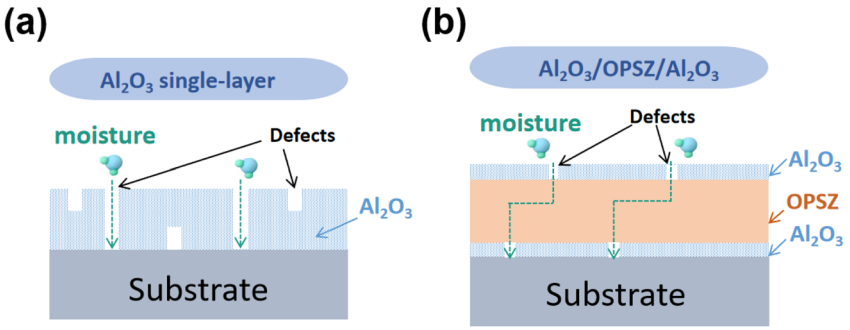

Fig. 10 Schematic of the diffusion of water vapor through the Al_2O_3 single-layer (a) and Al_2O_3/OPSZ/Al_2O_3 multilayer (b) films.

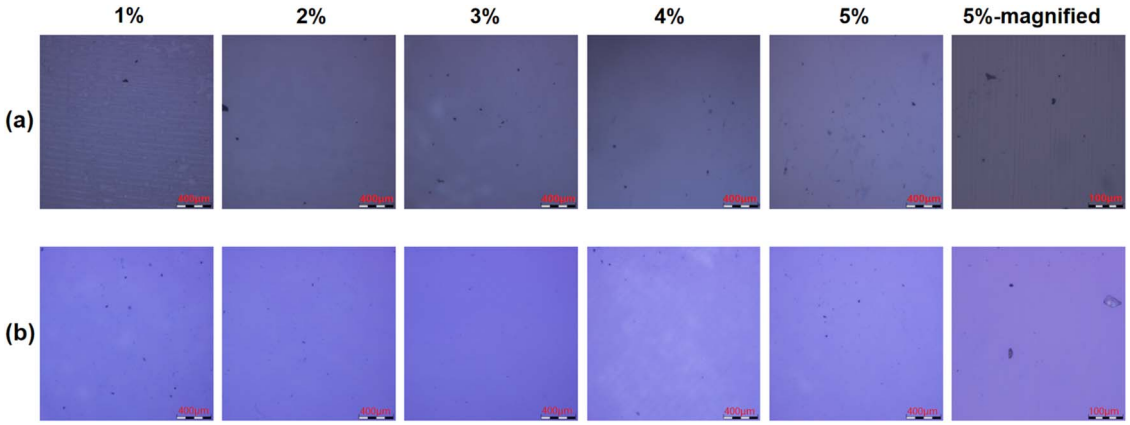

Fig. 11 Microscopic images for Al_2O_3 single-layer (a) and Al_2O_3/OPSZ/Al_2O_3 multilayer (b) films after 1%, 2%, 3%, 4%, and 5% tensile strain.

times are remarkably extended with a prolonged diffusion path of water vapor permeation owing to the presence of an organic layer sandwiched between the two Al_2O_3 inorganic layers.[34] Consequently, the Al_2O_3/OPSZ/Al_2O_3 multilayer film achieves significant barrier properties compared to the film made solely of Al_2O_3.

Tensile and bending strain measurements for 100 cycles are used to test the flexibility of barrier films. Fig. 11 shows that obvious cracks can be observed in the Al_2O_3 single-layer film when stretched at 5% strain, while no cracks are observed in the Al_2O_3/OPSZ/Al_2O_3 multilayer film with the applied strain from 1% to 5%. A bending test is performed

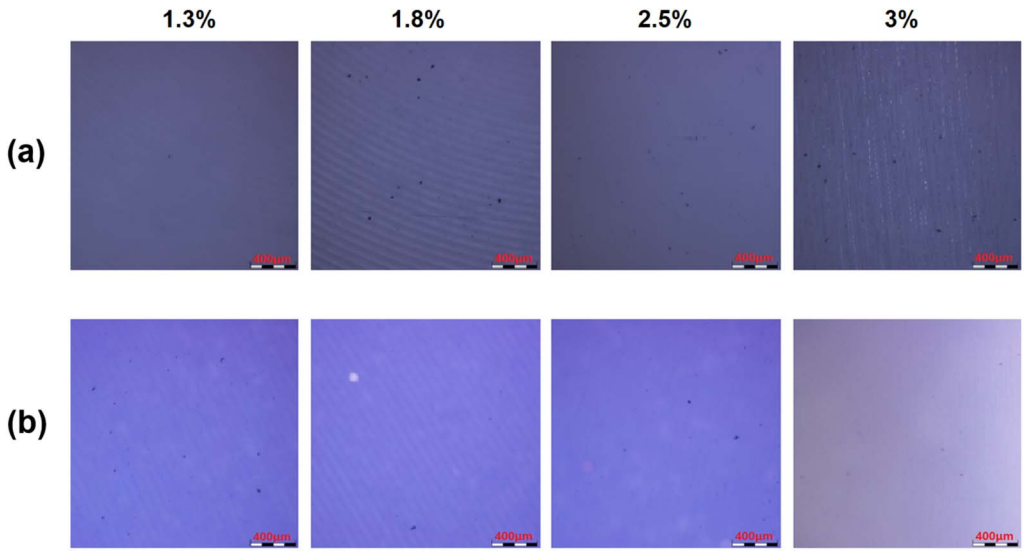

Fig. 12 Microscopic images for Al_2O_3 single-layer (a) and Al_2O_3/OPSZ/Al_2O_3 multilayer (b) films after 1.3%, 1.8%, 2.5%, and 3% bending strain.

with strains of 1.3%, 1.8%, 2.5%, and 3%. From Fig. 12, it can be observed that neither Al_2O_3 single-layer nor Al_2O_3/OPSZ/Al_2O_3 multilayer films show cracks at a low bending strain. Until the strain reaches 3%, cracks appear in the Al_2O_3 single-layer film. The above analysis indicates that the organic layer is advantageous for promoting the flexibility of barrier films. Therefore, the tensile and bending resistance of the Al_2O_3/OPSZ/Al_2O_3 multilayer film is better than that of the Al_2O_3 single-layer film.

The Al_2O_3/OPSZ/Al_2O_3 barrier film has potential value and wide application prospects in many industries, especially OLED and solar photovoltaic module encapsulation, which require a very high barrier grade for the encapsulation film. Furthermore, Al_2O_3 coatings have been used in a wide range of food packaging and bio-applications owing to their antibacterial and biocompatibility properties.[35,36] The Al_2O_3/OPSZ/Al_2O_3 barrier film, owing to its superior barrier performance, has greater potential for application in these fields.

4. Conclusions

In summary, Al_2O_3/OPSZ/Al_2O_3 multilayer barrier film on a 10 cm × 10 cm large-area PEN substrate is prepared using PEALD and spray-spin coating processes. The effects of fabrication parameters, layer number, and layer interaction on optical properties and microstructure are investigated systematically. Consequently, the fabricated multilayer film shows a smooth surface characteristic with a minimal R_a of 0.38 nm. Ultra-low WVTR value (4.6×10^{-5} g per m^2 per day, at 38 °C, 90% RH), high optical transmission (>90%), and good tensile and bending resistance are achieved. Thus, this work demonstrates that the fabricated multilayer structure barrier films possess great potential for the encapsulation of flexible devices.

Data availability

The raw data supporting the conclusions of this article will be made available by the authors upon request.

Author contributions

X. J. Sun: conceptualization, methodology, validation, formal analysis, investigation, writing—original draft preparation; W. Feng: writing-review and editing, supervision, project administration.

Conflicts of interest

There are no conflicts to declare.

Acknowledgements

This work was financially supported by the National Natural Science Foundation of China (Grant No. 52327802).

References

1 B. H. Kwon, H. Lee, M. Kim, C. W. Joo, H. Cho, J. T. Lim and Y. S. Jung, *J. Ind. Eng. Chem.*, 2021, **93**, 237–244.
2 Y. Li, K. Cao, Y. Xiong, H. Yang, Y. Zhang, Y. Lin, B. Zhou, J. Huang and R. Chen, *Adv. Mater. Interfaces*, 2020, **7**, 2000237.
3 Y. Weng, G. Chen, X. Zhou, Y. Zhang, Q. Yan and T. Guo, *ACS Appl. Polym. Mater.*, 2023, **5**, 10148–10157.
4 S. U. Shin and S. O. Ryu, *J. Electron.*, 2021, **50**, 2015–2020.
5 K. Y. Lim, H. H. Kim, J. H. Noh, S. H. Tak, J.-W. Yu and W. K. Choi, *RSC Adv.*, 2022, **12**, 4113–4119.
6 J. S. Park, H. Chae, H. K. Chung and S. I. Lee, *Semicond. Sci. Technol.*, 2011, **26**, 034001.
7 Q. Lu, Z. Yang, X. Meng, Y. Yue, M. A. Ahmad and W. Zhang, *Adv. Funct. Mater.*, 2021, **31**, 2100151.
8 Y. Weng, G. Chen, X. Zhou, Y. Zhang, Q. Yan and T. Guo, *ACS Appl. Polym. Mater.*, 2023, **5**, 10148–10157.
9 J. S. Lewis and M. S. Weaver, *IEEE J. Sel. Top. Quantum Electron.*, 2004, **10**, 45–57.
10 R. Q. Ma, R. Hewitt, K. Rajan, J. Silvernail, K. Urbanik, M. Hack and J. J. Brown, *J. Soc. Inf. Disp.*, 2008, **16**, 169–175.
11 Y. Leterrier, D. Pellaton, D. Mendels and R. Glauser, *J. Mater.*, 2001, **36**, 2213–2225.
12 Y. Li, Y. Xiong, H. Yang, K. Cao and R. Chen, *J. Mater.*, 2020, **35**, 681–700.
13 S. Lee, Y. Jeon, S. J. Oh, S.-W. Lee, K. C. Choi, T.-S. Kim and J. H. Kwon, *Mater. Horiz.*, 2023, **10**, 4488–4500.
14 S. J. Oh, S.-W. Lee, H. Lee, H. Kim, T.-S. Kim and J. H. Kwon, *Adv. Mater. Technol.*, 2024, **9**, 2400381.
15 M. Li, M. Xu, J. Zou, H. Tao, L. Wang, Z. Zhou and J. B. Peng, *Nanotechnology*, 2016, **27**, 494003.
16 J. Meyer, P. Görrn, F. Bertram, S. Hamwi, T. Winkler, H.-H. Johannes, T. Weimann, P. Hinze and P. Hinze, *Adv. Mater.*, 2009, **21**, 1845–1849.
17 A. Bulusu, A. Singh, C. Y. Wang, A. Dindar, C. Fuentes-Hernandez, H. Kim, D. Cullen, B. Kippelen and S. Graham, *J. Appl. Phys.*, 2015, **118**, 085501.
18 Y. Duan, Y. Q. Yang, Z. Chen, Y. Tao and Y. F. Liu, *Opt. Commun.*, 2016, **362**, 43–44.
19 P. F. Carcia, R. S. McLean and M. H. Reilly, *Appl. Phys. Lett.*, 2006, **89**, 031915.
20 M. S. Weaver, L. A. Michalski, K. Rajan, M. A. Rothman, J. A. Silvernail and J. J. Brown, *Appl. Phys. Lett.*, 2002, **81**, 2929–2931.
21 S. H. Jen and S. M. George, *ACS Appl. Mater.*, 2013, **5**, 1165–1173.
22 J. Parka, J. Setha, S. Chob and M. M. Sung, *Appl. Surf. Sci.*, 2020, **502**, 144109.
23 L. Sun, Y. Kurosawaa, H. Itob, Y. Makishimab, H. Kitab, T. Yoshidac and Y. Suzuri, *Org. Electron.*, 2019, **64**, 176–180.
24 P. van de Weijer, P. C. P. Bouten, S. Unnikrishnan, H. B. Akkerman, J. J. Michels and T. M. B. v. Mol, *Org. Electron.*, 2017, **44**, 94–98.
25 X. Wang, Y. H. Duan, Z. Chen, Y. Duan, Y. Q. Wang and P. Chen, *Nanoscale Res. Lett.*, 2015, **10**, 130.

26 S. A. Mahadik, F. Pedraza and S. S. Mahadik, *Prog. Org. Coat.*, 2017, **104**, 217–222.
27 Y. Q. Ren, X. J. Sun, L. L. Chen, H. Wei, B. Feng and J. Y Chen, *RSC Adv.*, 2023, **13**, 3766–3772.
28 E. J. Falde, S. T. Yohe, Y. L. Colson and M. W. Grinstaff, *Biomaterials*, 2016, **104**, 87–103.
29 N. Y. Garces, V. D. Wheeler and D. K. Gaskill, *J. Vac. Sci. Technol. B.*, 2012, **30**, 030801.
30 W. C. Shin, J. H. Bong, S. Y. Choi and B. J. Cho, *ACS Appl. Mater.*, 2013, **5**, 11515–11519.
31 K. L. Jarvis, P. J. Evans and G. Triani, *Surf. Coat. Technol.*, 2018, **337**, 44–52.
32 Q. Q. Chu, Z. Sun, D. Wang, B. Cheng, H. Wang, C. P. Wong and B. Fang, *Matter*, 2023, **6**, 3838–3863.
33 H. G. Kima, J. G. Leea and S. S. Kim, *Org. Electron.*, 2018, **52**, 98–102.
34 N. Kim, W. J. Potscavage Jr, A. Sundaramoothi, C. Henderson, B. Kippelen and S. Graham, *Sol. Energy Mater. Sol. Cells.*, 2012, **101**, 140–146.
35 V. Dias, H. Maciel, M. Fraga, A. C. Lobo, R. Pessoa and F. R. Marciano, *Materials*, 2019, **12**, 682.
36 J.-H. Eom, T.-Y. Cho and S.-K. Cho, *Appl. Surf. Sci.*, 2023, **638**, 158011.